Multi-scale roughness transfer in cold metal rolling

Franck Plouraboué, Matthieu Boehm

Multi-scale roughness transfer in cold metal rolling

Franck Plouraboué [c,*], Matthieu Boehm [a, b]

[a] *Laboratoire de Tribologie et Dynamique des Systèmes, Ecole Centrale de Lyon, UMR CNRS No. 5513, BP 163-69131 Ecully Cedex, France*
[b] *Péchiney Centre de Recherches de Voreppe, Centr'Alp, BP27, 38340 Voreppe, France*
[c] *Institut de Mécanique des Fluides, UMR CNRS No. 5502, Allée du Pr C. Soula, 31400 Toulouse, France*

Abstract

We report on a comparative Atomic Force Microscope (AFM) multi-scale roughness analysis of cold rolled Al alloy and steel roll, in order to characterize the roughness transfer from the steel roll to the workpiece in cold strip rolling processes. More than three orders of length-scale magnitudes were investigated from 100 microns to 50 nanometers on both types of surfaces. The analysis reveals that both types of surfaces are anisotropic self-affine surfaces. Transverse and longitudinal height profiles exhibit a different roughness exponent (Hurst exponent) $\zeta_\perp$=0.93±0.03 and $\zeta_\parallel$=0.5±0.05 Different length-scale cut-offs are obtained in each direction $l_\perp^{sup}$=50μm, $l_\parallel^{sup}\geq$100μm. Height and slope distributions are also computed to complement this study. The above mentionned self-affine characteresitics are found to be very similar for the roll and the strip surfaces, which suggest that roughness transfer takes place from the macroscopic (100 μm) to the very small scale (50 nm).

Keywords: Roughness; Self-affine; Rolling; Atomic Force Microscope

1. Introduction

Roughness conditions a number of properties of surfaces: optical (gloss, reflectivity, "surface aspect"), chemical (catalytic properties, corrosion,…) mechanical and tribological (load carrying capacity, friction, galling, adherence of coatings,…). More and more stringent roughness requirements are therefore imposed upon forming processes and finishing treatments of pieces, which implies that roughness must be measured accurately and related to processing conditions to be satisfactorily controlled. It has however been recognized that roughness is a multi-scale random process from the microscopic to the macroscopic scale, so that measured roughness numbers depend on the measurement length and profile discretization step [1–4]. This leads to an ever-increasing number of papers devoted to fractal characterization of surfaces, since the theory of fratal includes a multi-scale character and is thus able to explain scale-dependency of measurements, providing hopefully more intrinsic characteristics such as fractal dimension [5–13]. It has been applied to all kinds of engineering surfaces (from rock joints [14] via magnetic recording disk surfaces [15,7,8] to fractured surfaces [16–18]) obtained by almost any forming or finishing process (shaping and lapping [9]) electro-discharge machining [10], sand-blasting [12], rolling [19]. From an experimental point of view, various techniques have been used: mechanical profilometers [12,9,6], optical profilometers [7,8], optical interferometer [12,7], scanning tunneling microscopy [8], and Atomic Force Microscopy (AFM) [15,6]. All have their own limitations, but it is important to be able to investigate a sufficiently wide range of wavelengths.

The focus of the present paper is on rolled strips which may be sed for car body panels, metal packagings, and many other applications. In all cases, a certain level and morphology of roughness is to be obtained at the end of the rolling process for various reasons:

- Rolling may be a fast forming operation, with no surface finishing to be applied. The roughness created in the last rolling stands is then the final one and will control surface aspects and all surface properties.
- Rolling may be followed by further plastic processing (staming, deep drawing and ironing) during which the roughness created in the last rolling stands will gov-

* Corresponding author.

ern the friction and lubrication phenomena. Specific anti-galling roughness are thus imprinted in a special low rolling operation called skin-pass or temper-rolling.
- Even when further processing is present, the roughness created in the last rolling stands may remain on the final piece and control its properties: surface aspects and gloss (e.g stainless steel strips for domestic electric appliances), adhesion of coatings (galvanization and/or phosphating/painting of steel car body panel, tinning or varnishing of food or beverage cans,…) etc.

On the microscopic scale, obtaining a certain roughness on the strip is performed by transferring partly or totally the adequate roughness which has been sculpted on the rolls (by grinding, shot or sandblasting, electro-discharge machining, or electron beam texturing) via micro-plastic contact events such as:

- strip asperity flattening (to get a smoother and brighter strip)
- indenting or scratching of the strip surface by roll roughness asperities, complemented by the strip metal flowing into the roll surface valleys or grooves.

These micro-plastic processes are counteracted by the pressurized lubricant present between the roll and strip surface, in the scale range of the film thickness. Hydrodynamic lubrication may increase strip roughness ("orange peel") depending on the strip grain size and amount of deformation—a phenomenon which may be used to obtain certain surface morphologies. The multiscale nature of the obtained roughness might well be an important feature as far as such properties as brightness or adhesion of coatings are concerned, although such influences have not been documented yet to the best of our knowledge. On the other hand, it is well known that, as rolling and further forming operations are performed under a mixed regime, roughness has a very strong influence on lubricant flow and friction [20–22]. It is also established that for simple (Poiseuille [23,24]) flow configuration, the macroscopic hydrodynamic parameters such as permeability and percolation threshold [25] are dependent upon the multiscale character of roughness. It is therefore expected that lubrication of rolling and deep drawing are indeed influenced by roughness fractality.

We present here an extensive study of the multi-scale features of AFM images of industrially produced Al alloy sheets and steel rolls.

2. Experimental procedure

2.1. Atomic force microscopic measurements and characteristics

Topographic images have been achieved by means of a commercial AFM (Park Scientific) in contact mode using a long-range scanner (100 μm lateral travel and 5 μm vertical travel), in ambient air. Measurements were performed using a standard triangular cantilever (normal stiffness $\simeq$ 0.5 N/m) with a square pyramidal Si_3N_4 tip. The tip radius was about 50 nm. The scan rate has been chosen equal to 0.5 Hz for images of 512×512 data points. No image filtering was applied prior to the topographical analysis.

It is well known [26,27] that the tip shape limits the AFM resolution: an infinitely sharp tip is needed to get a perfect measure of surface roughness. This tip effect is increased for roughness length scales close to the tip radius. Many algorithms [28,29,26,27] have been proposed to remove the tip induced distortion. These reconstruction techniques need however the knowledge of the precise tip shape as indicated in Fig. 1. Unfortunately the tip geometry is generally not precisely known and may differ from one tip to another. Some authors [27,30] proposed therefore to get information about the tip structure from the analysis of the AFM image itself. This analysis needs however the existence of sharp surface features which are not present in the images studied here.

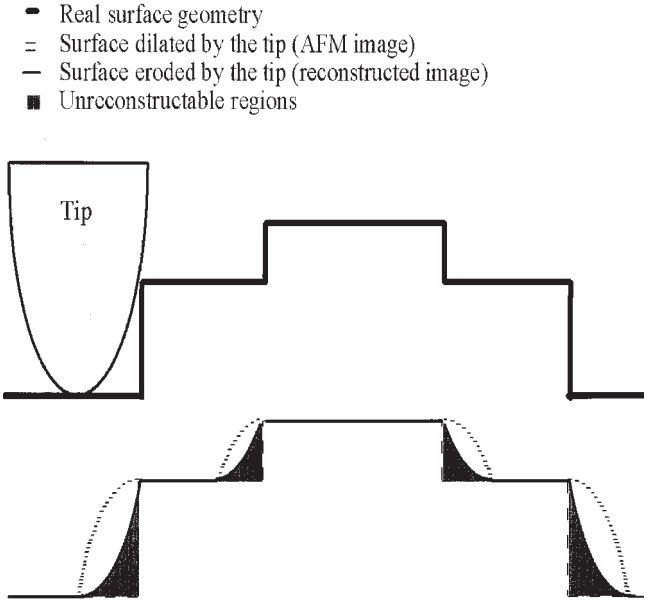

Fig. 1. Distorsions induced by the imaging of steps by a parabolic tip. The original profile can only be partially retrieved by the reconstruction technique. Bold solid lines of the upper step represent the real surface geometry, that cannot be imaged perfectly by the AFM tip. The AFM measured profile is sketched in the lower step, with dotted lines while the reconstructed profile is represented in bold. The grey zone, on the lower step represent the unreconstructable regions.

We therefore apply a standard isotropic reconstruction technique as described in [32] with a spherical tip radius ranging from 20–50 nm. Figs. 2a and b illustrate such reconstruction on a 1 μm^2 size. The distortions can be partially removed since, for any sample, there are some areas which do not come into contact with the tip. Hence, no image processing algorithm would be able to faithfully reconstruct these areas. At a larger scale however, the reconstruction leaves unchanged the measured images. The influence of the tip geometry on the following multi-scale analysis is estimated in the next section.

2.2. Sample description

We performed three series of measurements on three different classes of materials:

- (No. 1): rolled on industrial mill
- (No. 2): No. 1 further rolled (one pass) on a laboratory rolling mill. The samples were cut out from industrial aluminium alloy (Al 5182) rolling sheets. The Young modulus is equal to E=70 GPa, and a macroscopic root mean square (r.m.s) roughness respectively equal to σ_1=2.5 μm and σ_2=2.1 μm (along a 100 μm large window). The (No. 1) sheet is 600 μm thick and the (No. 2) is 420 μm (30% reduction).
- On a steel (AIS152100) roll (No. 3) is used for the additional rolling pass. The cylinder has a diameter equal to 400 mm and a roughness r.m.s σ_3=2.0 μm as described in [31]. The surface structure of this roll is very similar to those of the roll which has transformed sample No. 1 into No. 2, being obtained by the same grinding process with the same grinding wheels.

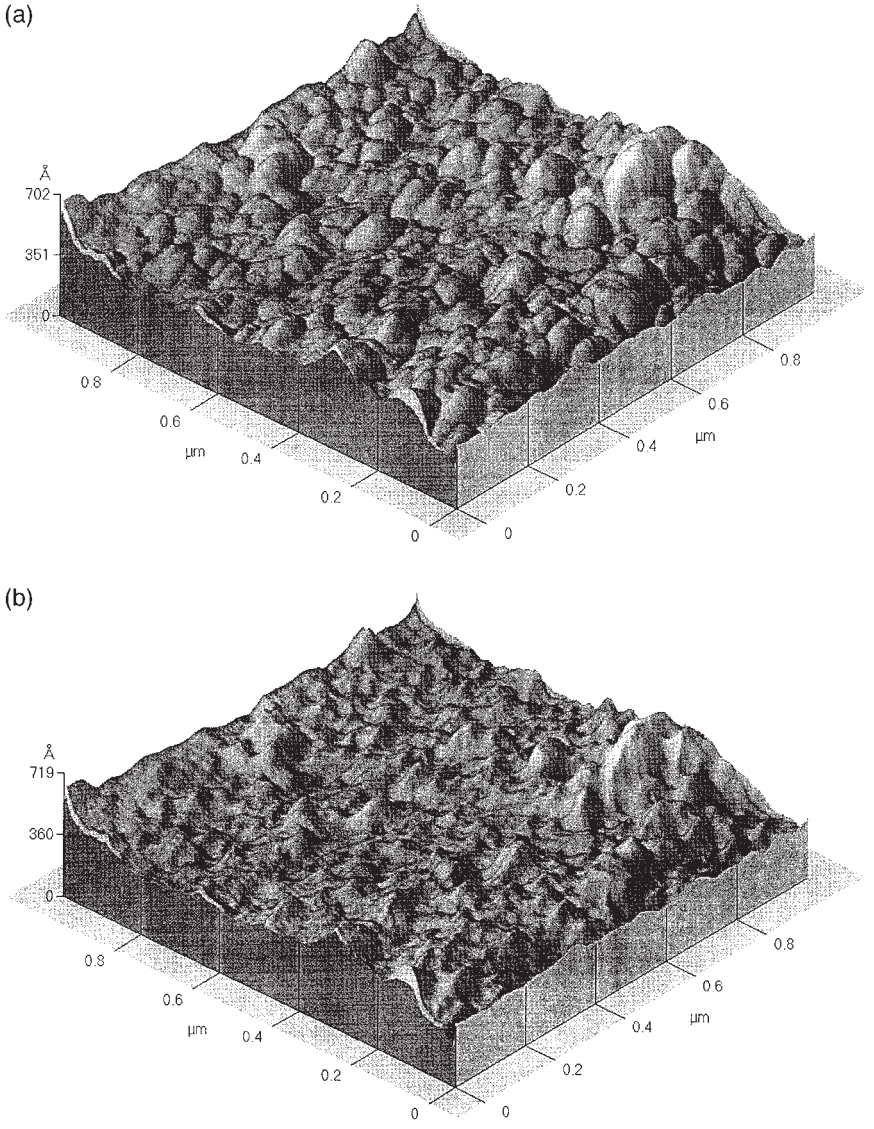

Fig. 2. AFM images of 512×512 points of the alloy sheet surface at 1 μm^2 scale. (a) direct image from AFM measurements; (b) reconstructed image for a given 30 nm AFM tip diameter.

The cylinders used for preceding rolling pass have larger diameters (close to 600 mm) but very similar surface roughness. Each sample has been rolled with a lubricating oil composed of a mixture of kerozine, lauric alcohol and isostearic acid. All samples were degreased with hexane before measurements. Their hardness and relative homogeneity allows simple and precise AFM measurements. Height maps were obtained with the fast scan direction parallel or perpendicular to the rolling direction. The misalignement between the rolling direction and the fast scan direction is about 0.02 radian. Hence, the AFM image is the superposition of different profiles obtained along the fast scan axis.

The topographical analysis has been achieved for different surface scales: 100×100 μm^2, 10×10 μm^2, and 1×1 μm^2, with a few nanometers precision in measured height and tens of nanometers on the horizontal position. In all cases maps $z(x,y)$ of 512×512 points have been recorded to analyze the roughness amplitudes from a few microns to a few nanometers. About one hundred such maps have been made in the course of our investigation.

3. Results

3.1. Qualitative topographical characteristics

Figs. 3a and b respectively show two examples of maps (No. 1) obtained at different scales (respectively 100×100 μm^2 and 10×10 μm^2). One can observe the characteristic anisotropy of such surfaces in the rolling direction. In the following we will refer to longitudinal direction—respectively transverse—for a direction parallel-respectively perpendicular—to the rolling direction. Transverse r.m.s roughness (perpendicular to the rolling direction) is five times larger than the longitudinal one. It is interesting to note that transverse roughness reveals different size distributions surimposed on the largest groove structures. Figs. 4a and b present similar views of roll topographical structure. The height dissymetry between the sheet in Fig. 3a and the roll in Fig. 4a is obvious: the roll surface Fig. 4a shows deep grooves on a rather flat surface and indeed has a negative skewness Fig. 5b, whereas the strip surface Fig. 3a has a positive skewness(Fig. 5a).

This complementary pre-dilection of alloy sheets for peaks and cylinder surface for holes is the signature of the plastic deformation during forming (indentation of the steel roll peaks and extrusion of the metal inside the cylinder roll ridges). We now investigate such roughness transfer at different length-scales.

3.2. Self-affine properties of anisotropic rough surfaces

Different techniques can be used for the analysis of multi-scale geometrical objects [21]. We focus our interest here on a mono fractal analysis which is less data consuming and gives a first description of the multi-scale characteristics of surface roughness. We will be mainly concerned in this study with anisotropic fractals named self-affine surfaces. Their major property is to be statistically unchanged under the general following rescaling

$$\begin{cases} x \rightarrow \lambda_1 x \\ y \rightarrow \lambda_2 y \\ z \rightarrow \lambda_3 z \end{cases} \quad (1)$$

where all different dilation ratios λ_i (i=1,2,3) only depend on one of them, say λ_3, chosen as a reference. Moreover since these transformations have a group structure, the dependence of λ_i (i=1,2) on λ_3 is through a homogeneous function [2]. This implies the existence of two independent scaling exponents, ζ_i for i=1 and 2 such that

$$\lambda_i = \lambda_3^{1/\zeta_i} \quad (2)$$

In the case of isotropic self-affine surfaces, x and y play a similar role and the exponent $\zeta_1=\zeta_2=\zeta$. In this case the ζ exponent is called the rough exponent or the Hurst coefficient and is simply related to the fractal dimension D of one profile by $\zeta=2-D$. In the more general case considered in this study, we will refer to x as the longitudinal direction with associated exponent $\zeta_\parallel$ and to y as the transverse direction with exponent $\zeta_\perp$. Hence the invariance can be rewritten:

$$\begin{cases} x \rightarrow \lambda^{1/\zeta_\parallel} x \\ y \rightarrow \lambda^{1/\zeta_\perp} y \\ z \rightarrow \lambda z \end{cases} \quad (3)$$

Hence each extracted profile of the surface along x—resp. y—direction will be self-affine with rough exponent $\zeta_\parallel$—resp. $\zeta_\perp$ In the following, we will focus on the statistical property of the covariance function $C(\vec{\Delta})$—also called the structure function:

$$C(\vec{\Delta}) = \langle (z(\vec{x}) - z(\vec{x}+\vec{\Delta}))^2 \rangle \quad (4)$$

where the average <…> is taken over x and y, and $\vec{\Delta}$ is a vector in the Oxy plane. Statistical invariance Eq. (3) implies that the covariance satistics: $C(\lambda_\perp \vec{\Delta}_\perp) = (\lambda_\perp^{2\zeta_\perp}) C(\vec{\Delta}_\perp)$ for positive $\lambda_\perp$ and the same in x direction for $\lambda_\parallel$.

This property implies that the scaling dependence of the covariance function Eq. (4) in both direction x and y verifies:

$$C(\vec{\Delta}_\parallel) = A_\parallel \Delta_\parallel^{2\zeta_\parallel}, \; C(\vec{\Delta}_\perp) = A_\perp \Delta_\perp^{2\zeta_\perp} \quad (5)$$

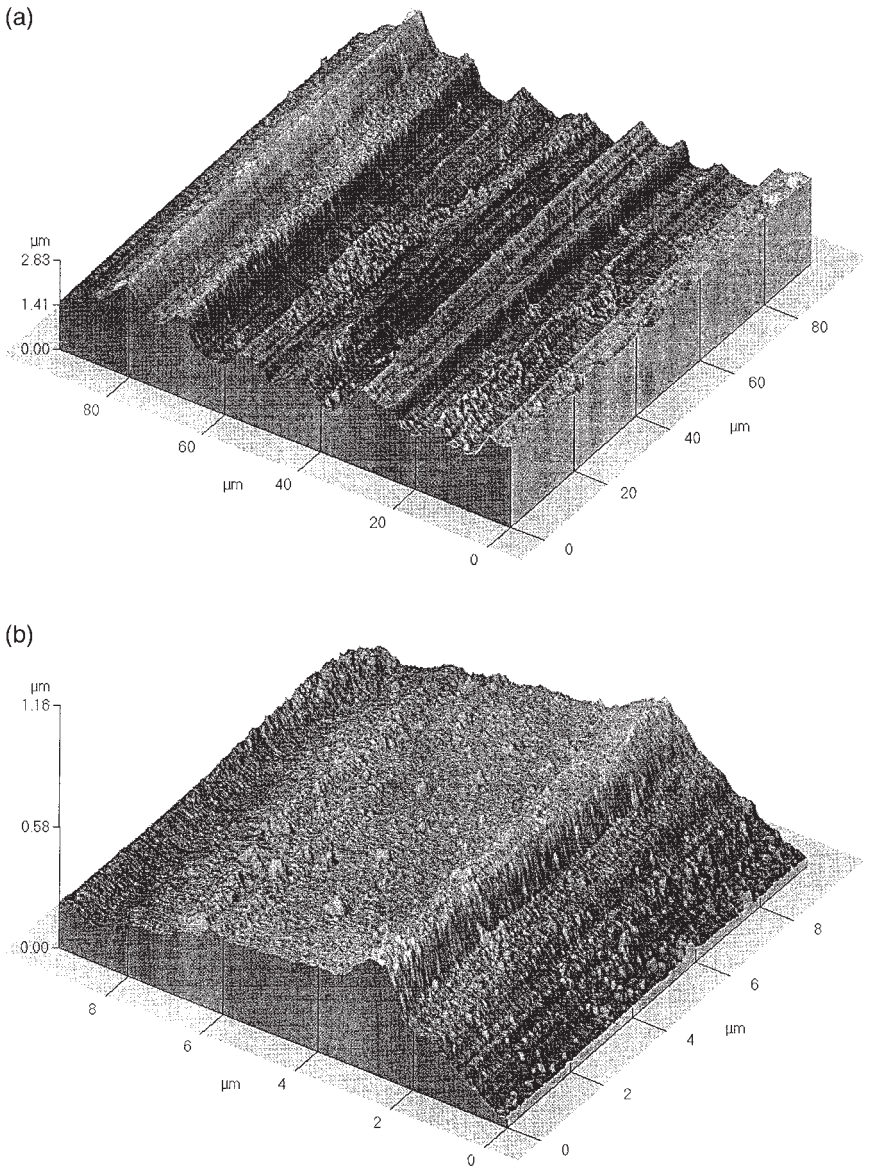

Fig. 3. AFM images of 512×512 points of the alloy sheet surface. (a) at 100 μm² scale; (b) at 10 μm² scale.

where $A_\perp$ and $A_\parallel$ are called the roughness amplitude coefficients.

The most standard method used to study the correlation function dependence with the examined scale is to compute the power spectrum. From the Fourier transform $\tilde{z}(\vec{k})$ of the profiles $z(\vec{x})$, one can easily compute the spectrum $P(\vec{k})=|\tilde{z}(\vec{k})|^2$. The power spectrum coincides—except at the origin k=0—with the Fourier transform of the correlation function $P(\vec{k})=|\tilde{z}(\vec{k})|^2=z\bigstar z=C(\vec{\Delta})$ because of the simple property of Fourier transform related to the convolution products ★. When the correlation function displays a power law behavior Eq. (5) as for self-affine profiles, it can be shown that the power spectrum scales as:

$$P(\vec{k}_\parallel)\propto A_\parallel K_\parallel^{-1-2\zeta_\parallel},\ P(\vec{k}_\perp)\propto A_\perp K_\perp^{-1-2\zeta_\perp} \quad (6)$$

Hence averaging $P(k)$ over different profiles preserves the scaling and allows for a more precise determination of the exponents.

3.3. Data analysis, sampling effects, disorientation effects

We consider each direction independently and the linear drift of each profile—e.g $z(x,0)$—is set to zero—e.g $z(0,0)=z(L,0)=0$, where L is the total length of the profile. Fig. 6a shows the superposition of averaged power spectrum obtained from 5×512 transverse profiles of length L=512 extracted from 15 surfaces of 100×100 μm², 10×10 μm²and 1×1 μm² of sheet samples of type (No. 1). Fitting the spectrum by a power-law—dotted line—as expected if the profiles are self-affine, provides the

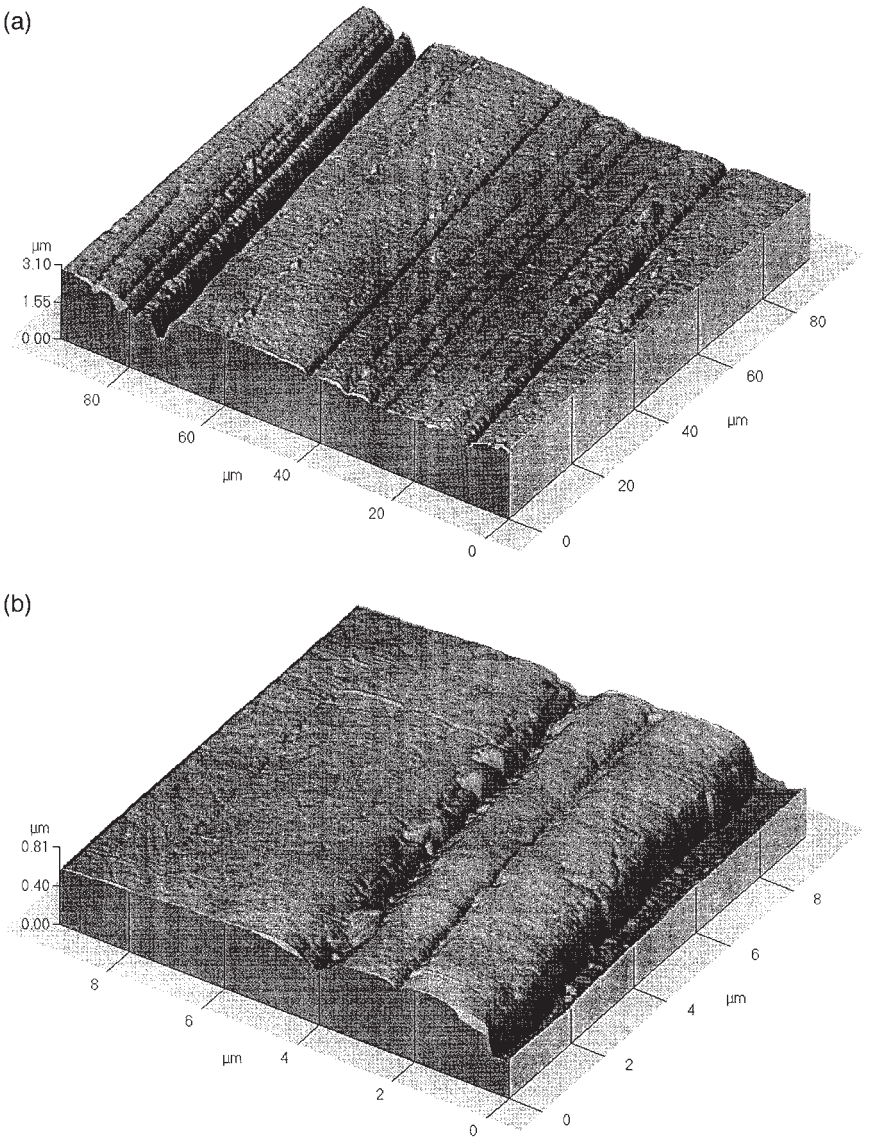

Fig. 4. AFM images of 512×512 points of the steel cylinder surface. (a) at 100 μm^2 scale; (b) at 10 μm^2 scale.

estimate of the transverse roughness exponent. A good self-affine behavior is found over almost three decades from which a transverse exponent can be estimated: $\zeta_\perp$=0.93±0.03. This scaling law can be applied from large length scale (50 μm) to small ones (50 nm). Fig. 6b illustrates the same property in the longitudinal direction, from which a longitudinal rough exponent is estimated $\zeta_\parallel$=0.4±0.05 over almost three orders of magnitude between 100 μm and 200 nm. At a small scale the comparison of Figs. 6a and b indicates a similar behavior, and thus an isotropy of the roughness structure at small scale. It is however questionable that such isotropy may be an artifact of the AFM measure which is known to induce distortion at a small scale.

This question is addressed using the reconstruction technique discussed in the previous section. Fourier spectra of both original and reconstructed 1 μm^2 surfaces has been computed for 20–50 nm tip radius—as represented on Fig. 7 in the case of 30 nm. These chosen tip radii are consistent with the known geometrical characteristics of the AFM. real tip. Reconstructed power spectra remain isotropic, i.e the measured roughness amplitude and exponent in the transverse and longitudinal directions are very similar up to finite size effects. Moreover the main feature of reconstruction is indeed to erase a small scale peak. We can thus associate this small scale spectrum peak to the geometrical image deformation coming from the AFM tip as illustrated in Fig. 1. Moreover the length scale also cited with the small scale spectrum peak in Fig. 7 is consistant with the tip radius size (20–50 nm). From the assumption, coming from the reconstruction technique, that the spectrum peak is associated with the tip distortion, we can thus get from this length scale, an estimate of the tip radius.

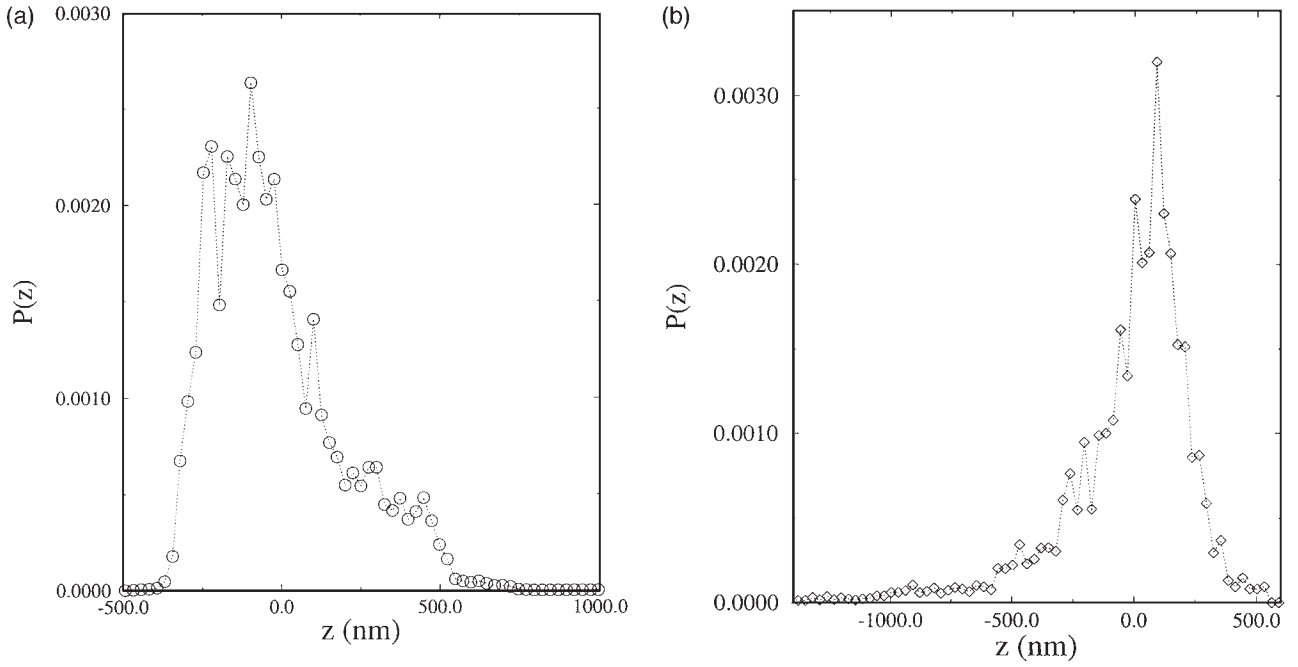

Fig. 5. Height distribution is computed from averaging five 100 μm² surfaces of 512× 512 points. (a) ○ for alloy sheet sample (2) being rolled-pass by the cylinder; (b) ◇ for steel roll.

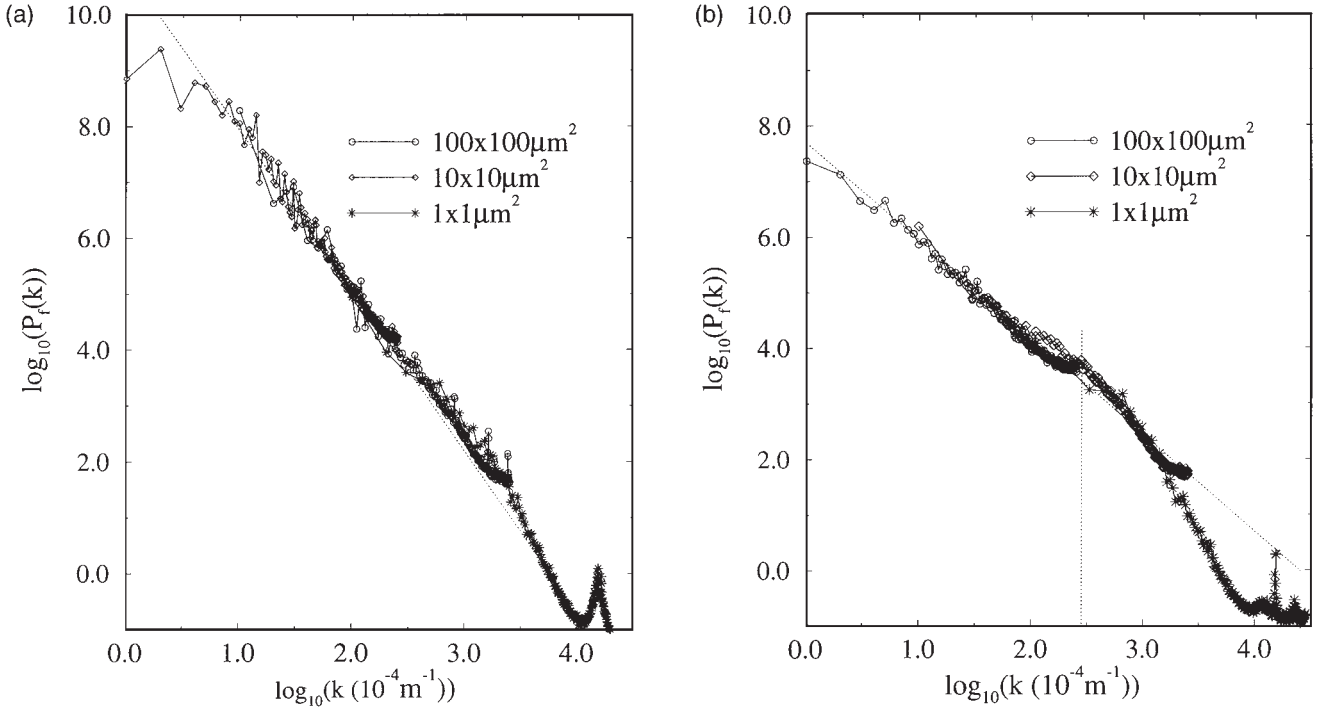

Fig. 6. Averaged power spectra of height profiles of the Al alloy sheet (No. 1) in log-log coordinates at different scales: ○ 10 μm, ◇ 10 μm, and ★ 1 μm. Dotted line indicates self-affine power law. (a) In transverse direction : the estimated transverse self-affine exponent is $\zeta_{\perp}$=0.93±0.05; (b) In longitudinal direction : $\zeta_{\parallel}$=0.4±0.1.

This treatment confirms the validity of the small scale AFM measures and associates the small scale peak to a spurious measure artefact. Hence we keep the following original AFM data for the multi-scale analysis.

Fig. 8 shows the superposition of the average power spectra realized on (No. 2) sheets for transverse and longitudinal directions with the same conditions as in Figs. 6a and b. Estimated transverse rough exponent

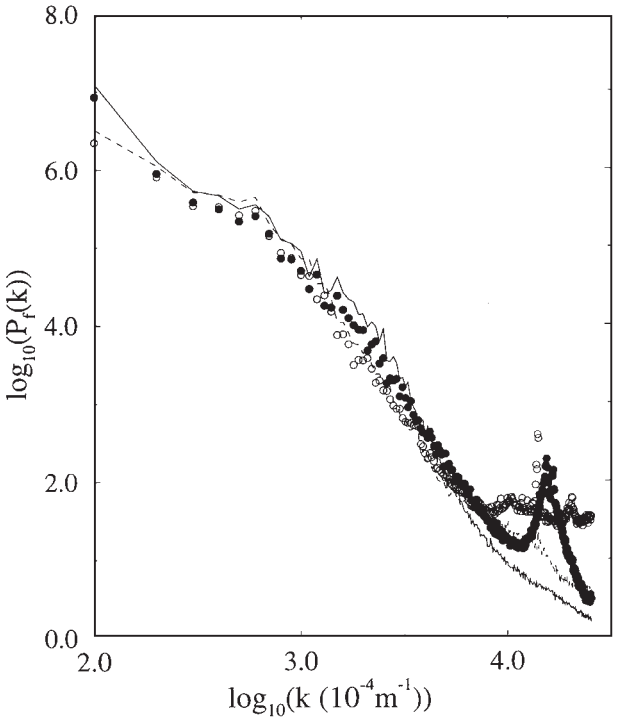

Fig. 7. Comparison of height power spectra between direct and eroded images of 1 μm^2 size. Averaged power spectrum of 512 height profiles is shown in log-log coordinates for real data in transverse ● and longitudinal ○ directions, as well as for reconstructed profiles with full line in the transverse direction and dashed line in the longitudinal direction.

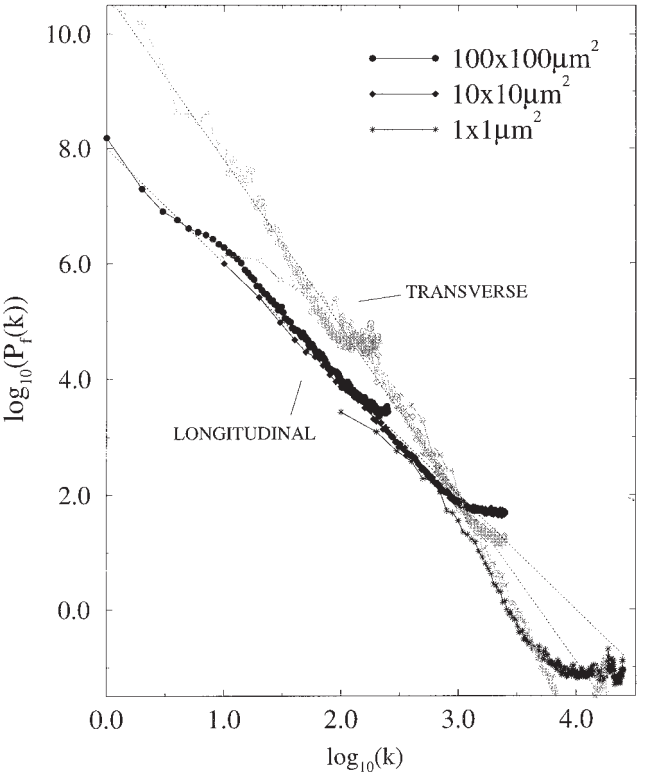

Fig. 8. Same conventions as Fig. 6 for the Al alloy sheet (No. 2). In transverse direction with grey points: $\zeta_\perp$=0.93±0.05 In longitudinal direction black points: $\zeta_\parallel$=0.5±0.1.

$\zeta_\perp$=0.93±0.03 is very similar to the one computed for the type (No. 1) sheet, whereas the longitudinal rough exponent is slightly higher, $\zeta_\parallel$=0.5±0.05. The upper and lower cut-off of the power law are very close to the type (No. 1) sample. Fig. 9 displays the roll (No. 3) power-spectra—same conditions as Fig. 8. Here again the transverse multi-scale characteristics are very similar to those observed in Figs. 6a and 8. The transverse rough exponent estimation $\zeta_\perp$=0.95±0.03 of steel roll (No. 3) is very similar to the (No. 1) and (No. 2) ones. The cut-off length scales estimations are very close to 50 µm and 50 nm as for sample (No. 1). In the longitudinal direction the estimated rough exponent $\zeta_\parallel$=0.6±0.05 is again slightly higher than for sample (No. 2)—cf Fig. 8. The isotropy length scale for which transverse and longitudinal directions behave similarly appears to be very close to 200 nm on all samples; (No. 1), (No. 2) and (No. 3).

All these observations agree with the presence of roughness transfer even at very small scale. The intermediate value of the longitudinal rough exponents of samples (No. 2), between the values of samples (No. 1) and (No. 3) is also consistent with a multiscale roughness transfer. One rolling-pass of the sheet (No. 1) seems to modify the surface structure in the longitudinal direction. It is however questionable whether the small difference between longitudinal exponent of samples (No. 1), (No. 2) and (No. 3) could be due to some sampling effect.

This motivates the use of another multi-scale analysis technique to better define the error bars of the estimated exponent. We used the variable band-width method which consists of dividing a given profile of length L in windows of width Δ. Although this method is more sensitive to finite size effects [1]—i.e the estimated rough exponents are more sensitive to the length size L of examined profiles than the power spectrum—they provide complementary estimates for rough exponents and their error bars. A complete analysis of the sample size influence on self-affine exponent estimation can be found in Ref. 1. The method consists in computing the r.m.s roughness σ and the difference δ between the maximum and minimum height on each window, and averaging over all windows of given width Δ covering the total length L, $(\sigma)_\Delta$ and $(\delta)_\Delta$. Window sizes larger than $L/2$ are discarded because of insufficient independent sampling. Both variables, in the case of self-affine profiles, follow the simple scaling :

$$(\sigma)_\Delta \propto \Delta^\zeta \quad (7)$$

$$(\delta)_\Delta \propto \Delta^\zeta \quad (8)$$

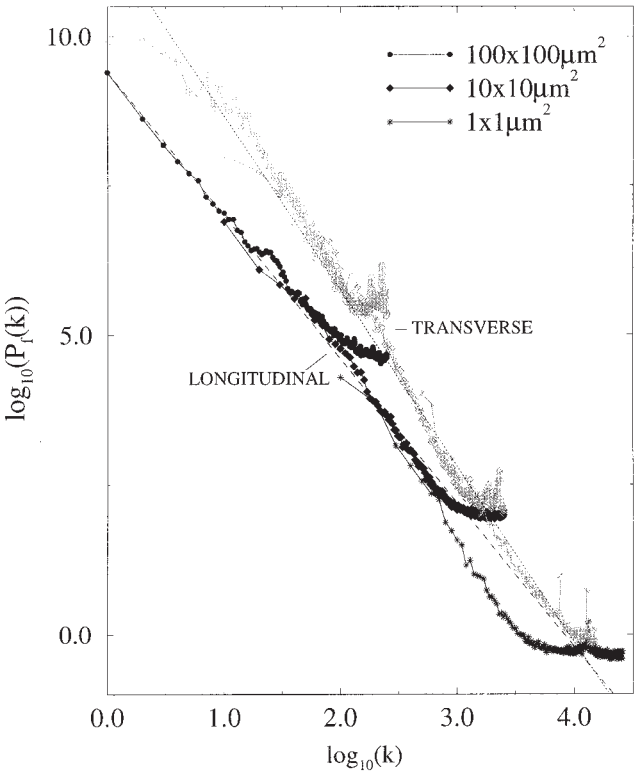

Fig. 9. Power spectra of the steel cylinder with the same conventions as Fig. 8 in both transverse and longitudinal directions. Estimation of rough exponent is, in transverse direction, $\zeta_\perp$=0.95±0.05, while in longitudinal direction $\zeta_\parallel$=0.6±0.1.

Where ζ is the rough exponent corresponding to the examined direction (transverse or longitudinal). Figs. 10a and b illustrate such scaling for 5×512 different averaged profiles extracted from 100 μm^2 and 10 μm^2 surfaces and confirm the previous estimates of rough exponents in both directions. Moreover Fig. 10a shows a saturation of the scaling Eq. (7) in the transverse direction. This indicates, as already mentioned with the power spectrum analysis of Fig. 6a, the existence of an upper cut-off of the self-affine scaling Eq. (7) close to 50 μm. Comparison between Figs. 10a and b reveals that the longitudinal upper cut-off is probably larger than 50 μm^2. One can estimate the anisotropy roughness ratio between the "large scale" (L=50 μm) r.m.s roughness in transverse and longitudinal directions is close to $\sigma_{1\perp}/\sigma_{1\parallel}\simeq 8$. This measure allows the determination of amplitude coefficients $A_\parallel$ and $A_\perp$. The same observation is valid for sample (No. 2) as illustrated in Fig. 11. Comparison between Figs. 10a and 11 of the transverse "large-scale" r.m.s roughness indicates a small roughness reduction from $\sigma_{1\perp}$=2.5 μm for sample (No. 1) to $\sigma_{2\perp}$=2.1 μm for sample (No. 2), as already mentioned. All these characteristics of the strips are consistent with a roughness transfer from the steel roll analysis of Fig. 12. Roughness amplitudes in both transverse and longitudinal directions, the anisotropy ratio of the "large-scale" roughness and longitudinal cut-off are common features of strip sample (No. 2) and steel roll (No. 3). Quantitative estimates are reported in Table 1.

Hence the variable band width method has confirmed the spectrum analysis as well as estimated the roughness amplitudes. It has also provided a better estimate of the rough exponents error bars due to finite size effects. Nevertheless another possible source of errors in the rough exponent estimation is the small disorientation ϵ of measured surfaces with the real rolling direction—as can be observed in Fig. 2a where $\epsilon\simeq 0.02$. As the extracted profiles are not exactly parallel—resp. perpendicular—to the rolling direction, the estimation of one exponent can be influenced by the other one. This error is much larger in longitudinal than in transverse direction because transverse roughness amplitude is much larger than the longitudinal one. The estimated roughness $\sigma_\parallel$ of extracted profiles is the sum of both contributions from the true longitudinal and transverse directions:

$$\sigma_\parallel(L)=A_\parallel L^{\zeta_\parallel}\simeq\sigma_\parallel^\star(L)+|\epsilon|\sigma_\perp^\star(L)\simeq A_\parallel^\star L^{\zeta_\parallel^\star} \quad (9)$$
$$(1+|\epsilon|(A_\perp^\star/A_\parallel^\star)L^{\zeta_\perp^\star-\zeta_\parallel^\star})$$

Where superscript ★ represents the real value corresponding to ϵ=0. Eq. (9) indicates that both estimated roughness exponent $\zeta_\parallel$ and amplitude $A_\parallel$ are systematically increased by the disorientation. Moreover the second term of the left hand size of Eq. (9) reveals that disorientation effect is much sensitive at large scale because $\zeta_\perp^\star-\zeta_\parallel^\star>0$ in our case. Using Eq. (9) and values of Table 1 we compare the estimated variable band width roughness $\sigma_\parallel(L)$ with its correction $\sigma_\parallel^\star(L)$ in Fig. 13 using ϵ=0.05 and $^\star_\perp-\zeta_\parallel^\star$=0.3–0.5. The estimated rough exponent is only weakly influenced, up to a few percent—i.e. the slope is weakly modified. We can deduce from this analysis, new error bars reported in Table 1 for the roughness exponent estimation. On the other hand the roughness amplitude can be markedly enhanced at a large scale by the disorientation effect. One can estimate from Eq. (9) the error committed on the estimation of the roughness amplitude: $(A_\parallel-A_\parallel^*)/A_\parallel\simeq\epsilon(A_\perp^*/A_\parallel)L^{\zeta_\perp^*-\zeta_\parallel}$. The disorientation effect is very weakly affecting the transverse direction, hence, very good estimates of $A_\perp^\star$ and $\zeta_\perp^\star$ are $A_\perp$ and $\zeta_\perp$. It is then possible to estimate the error committed on the longitudinal amplitude $A_\parallel$ at large scale L=50 μm from values of Table 1, and for ϵ=0.05: $(A_\parallel-A_\parallel^*)/A_\parallel\simeq 0.35$. Hence, due to the measured AFM images disorientation, transverse roughness amplitude estimation can be 35% overestimated in Table 1.

This analysis of the errors committed on the estimation of parameters leads to the conclusion that (i) the longitudinal exponent $\zeta_\parallel$ is significantly different on the three samples (No. 1), (No. 2) and (No. 3) and that (ii)

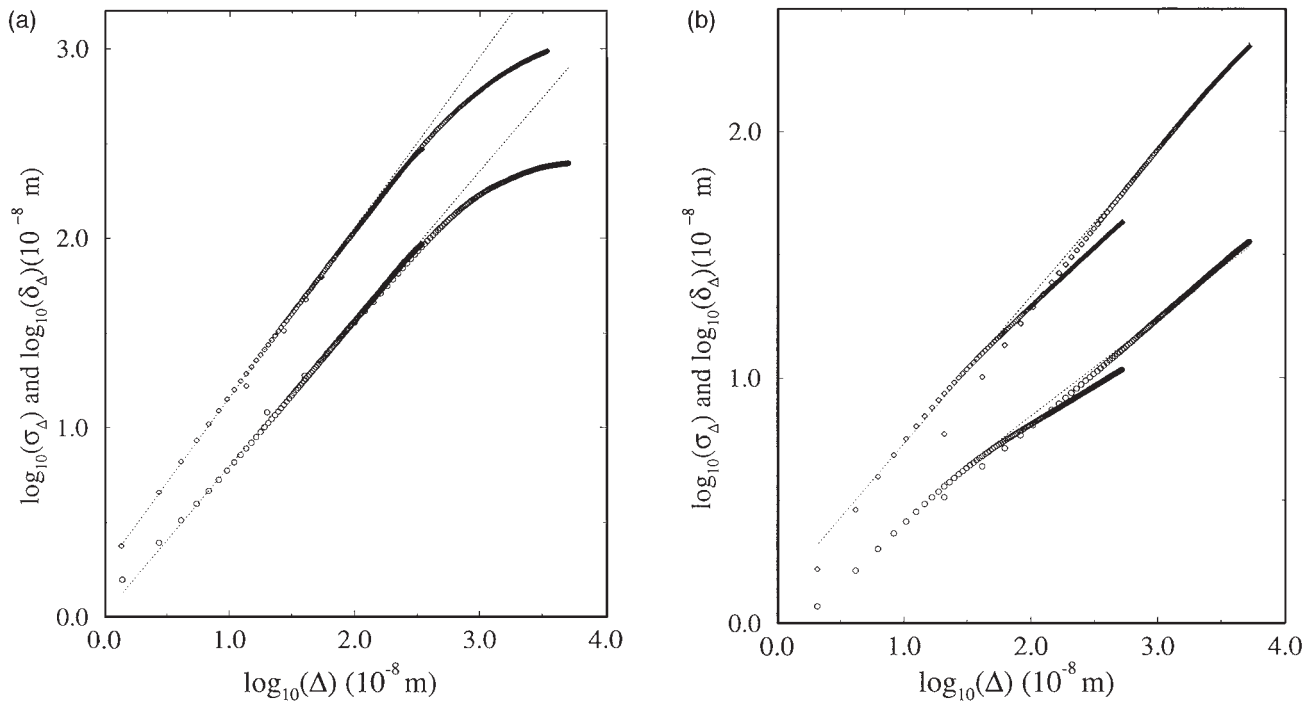

Fig. 10. Variable band width method is used to analyze the height profile of the alloy sheet sample (No. 1). ◇ Root mean square deviation σ and ○ min-max difference are plotted versus the window size Δ in log-log coordinates (a) In transverse direction: $\zeta_\perp$=0.85±0.07; (b) In longitudinal direction: $\zeta_\parallel$=0.5±0.1.

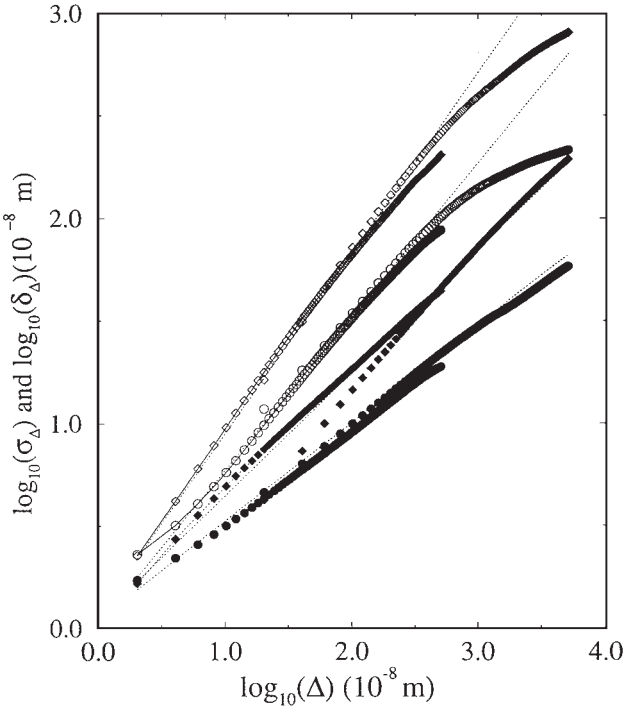

Fig. 11. Variable band width method is used to analyze the alloy sheet sample (No. 2) with the same conventions as Fig. 10 with white symbols in transverse direction and black symbols in the longitudinal one. (a) In transverse direction: $\zeta_\perp$=0.85±0.07; (b) In longitudinal direction: $\zeta_\parallel$=0.55±0.08.

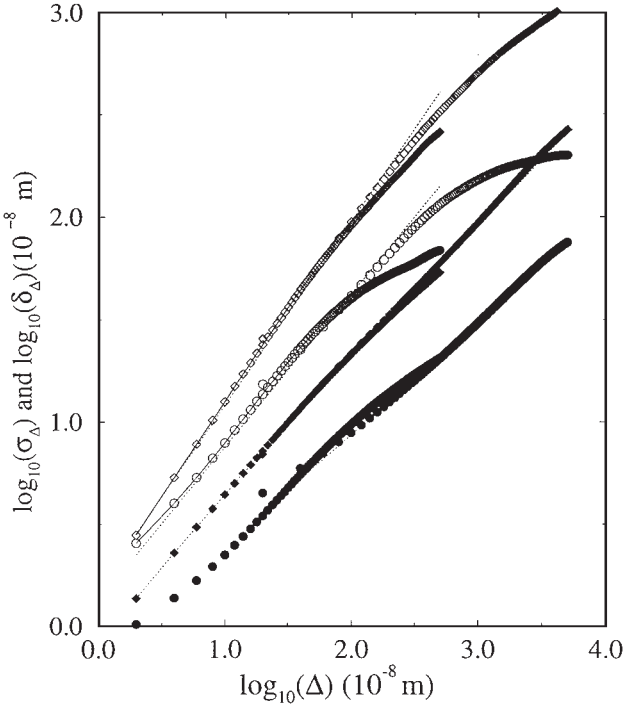

Fig. 12. Variable band width method is used to analyze the steel cylinder sample (No. 3) with the same conventions as Fig. 11. Estimate exponents are $\zeta_\perp$=0.85±0.07 and $\zeta_\parallel$=0.6±0.5.

Table 1
Measured roughness exponent and roughness amplitudes with estimated error bars

	$\zeta_\perp$	$\zeta_\parallel$	$\sigma_\perp(L{=}50\ \mu m)$
Al alloy sheet (No. 1)	0.93±0.05	0.4±0.1	2.5 μm
Al alloy sheet (No. 2)	0.93±0.05	0.5±0.1	2.1 μm
steel roll (No. 3)	0.95±0.08	0.6±0.1	2.0 μm
	$\sigma_\parallel(L{=}50\ \mu m)$	$A_\perp$	$A_\parallel$
Al alloy sheet (No. 1)	0.3 μm	0.066 $\mu m^{0.07}$	0.062 $\mu m^{0.6}$
Al alloy sheet (No. 2)	0.5 μm	0.055 $\mu m^{0.07}$	0.07 $\mu m^{0.5}$
steel roll (No. 3)	0.7 μm	0.052 $\mu m^{0.05}$	0.077 $\mu m^{0.4}$

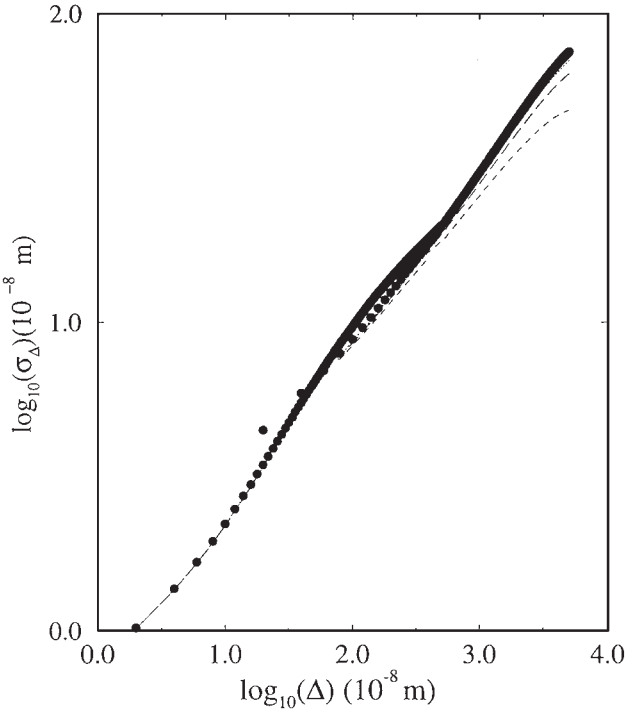

Fig. 13. Correction to the disorientation effect is computed for the r.m.s roughness $\sigma_\parallel(L)^\star$—dashed lines—from Eq. (9) with ϵ=0.05 and previously measured $A_\perp$ and $A_\parallel$. These corrections are compared to the previously computed variable band width longitudinal roughness ● $\sigma_\parallel(L)$ of Fig. 12. Corrections corresponding to $\zeta_\perp^\star - \zeta_\parallel^\star$ 0.3, 0.4 and 0.5 are superposed with the ● data, with respectively dotted, long dashed, and dashed lines.

the longitudinal roughness amplitude can be quite largely affected by disorientation effects.

3.4. Slope analysis

The analysis of slope distribution on both rolled sheet surfaces and steel roll is important for the hydrodynamics of metal forming. It can indeed be shown that the Reynolds approximation can be used to describe the fluid behavior as far as local slopes of both roll and sheet remain small [32].

Fig. 14 displays the slope histogram computed from five measured (No. 1) sheet surfaces of 100×100 μm^2 and five of 10×10 μm^2 in both transverse and longitudinal directions. We extract the square root of the slope variance $\sigma(\theta)$ of these distributions in order to obtain the typical slope. Because of the self-affine structure of these surfaces the typical slope is growing up when the observation scale l is decreasing. It is possible to evaluate, at a given scale l, the typical slope $\sigma(\theta)$. The r.m.s roughness at a scale l, is Al^ζ which is equal to the height due to the typical slope $l\tan(\sigma(\theta))$. This leads to the following scaling of the typical slope:

$$\tan(\sigma(\theta)) \propto l^{\zeta-1} \tag{10}$$

Table 2 summarizes the typical slopes obtained in both transverse and longitudinal directions, at two different scales of measure $l \simeq 200$ nm and 20 nm for sheet and roll surfaces. We first note that all observed slopes remain small, as generally observed on manmade metal surfaces. Comparison between expected—from Eq. (10) and observed ratio of typical slope $\sigma(\theta)_l/\sigma(\theta)_{l/10}$ at different scales are detailed in Table 2. This comparison indicates that both estimates of slopes from direct measurements or from previous estimations of roughness exponents through Eq. (10) are very close. The slope analysis is thus consistent with the previous self-affine analysis of the surface roughness.

4. Conclusion

This study investigates, using AFM measurements, the self-affine character of rolled strip surfaces. It is demonstrated that both rolled aluminium alloy sheet and roll surfaces are anisotropic self-affine surfaces with very similar features. We estimate in both transverse and longitudinal directions rough exponents and amplitudes. While transverse characteristics are very close we note a difference between longitudinal rough exponents of sheets and roll. Moreover we observe that this difference is reduced by a rolling pass. This observation leads us to the conclusion that the roughness transfer affects the

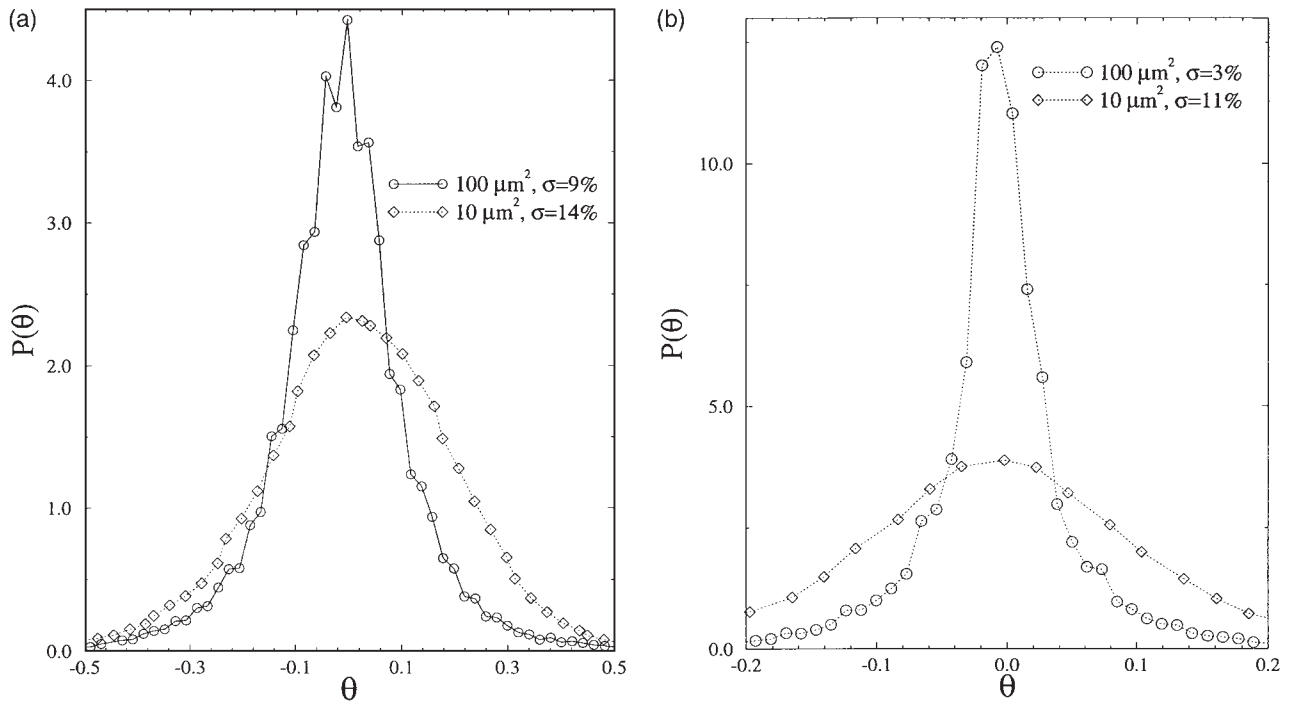

Fig. 14. Slope histogram for alloy sheets of type (No. 1) (a) in transverse direction ○ at l=100/512≃0.2 μm scale, ◇ at l=10/512≃0.02 μm scale; (b) in longitudinal direction, same conventions as (a).

Table 2
Typical measured slopes $\sigma(\theta)$ at different scales l=20 nm and l/100 along transverse and longitudinal directions

	$\sigma(\theta)_{\parallel}(l)$	$\sigma(\theta)_{\parallel}(l/10)$	$\sigma(\theta)_{\perp}(l)$	$\sigma(\theta)_{\perp}(l/10)$
Al sheets	0.03	0.11	0.09	0.14
steel roll	0.06	0.16	0.09	0.12
	$\sigma(\theta)_{\parallel}(l)/\sigma(\theta)_{\parallel}(l/10)$	$\sigma(\theta)_{\parallel}(l)/\sigma(\theta)_{\perp}(l/10)$ estimated from Eq. (10)	$\sigma(\theta)_{\perp}(l)/\sigma(\theta)_{\perp}(l/10)$	$\sigma(\theta)_{\perp}(l)/\sigma(\theta)_{\perp}(l/10)$ estimated from Eq. (10)
A1 sheets	0.28	0.27	0.64	0.75
steel roll	0.37	0.39	0.75	0.75

multi-scale properties of formed surfaces in both transverse and longitudinal directions. Moreover both types of surfaces display at a small scale a common self-affine isotropic roughness. Hence roughness transfer occurs even at very small scales of the order of 50 nm. The measured surface slopes remain small in all directions. Moreover, as expected with self-affine surfaces, the slopes increase when decreasing the observation length scale.

Acknowledgements

This work was supported by the Research project contract (CPR) “Mise en forme des matriaux : Contact outilmtaJ- lubrifiant” between CNRS (SCA), Irsid (Usinor Group), Pchiney centre de recherche de Voreppe, Paris Sud Orsay University (LMS), College de France (PMC), ECL (LTDS), INPT (IMFT), INSA. de Lyon (LMC), ENSMP (CEMEF). We acknowledge the help of Pchiney Recherche centre de recherche de Voreppe for exper imental and technical support. We give thanks to M. Prat, P. Montmitonnet, M. Guttmann and P. Deneuville for their remarks and careful reading of the manuscript.

References

[1] Schmittbuhl J, Vilotte JP, Roux S. Phys Rev E 1995;51:131.
[2] Feder J. Fractals. New York: Plenum Press, 1988.
[3] Brown CA. Int J Mach Tools Manufact 1998;38:633.
[4] Dong WP, Mainsah E, Stout KJ. Int J Mach Tools Manufact 1996;36:1347.
[5] Suryaprahash S, Bhushan B. Wear 1995;180:17.
[6] Poon CY, Bhushan B. Wear 1995;190:76.
[7] Mahumdar A, Tien CL. Wear 1990;160:313.
[8] Yang M, Talke F. Wear 1993;170:15.
[9] He L, Zhu J. Wear 1997;208:17.
[10] Zhou G, Leu MC, Blackmore D. Wear 1993;170:1.
[11] Yordanov OI, Ivanova K. Surface science 1990;331-333:1043.

[12] Gagnepain J, Roques-Carmes C. Wear 1986;109:119.
[13] Lee SH, Zahouani H, Caterini R, Mathia T. Int J Mach Tools Manufact 1998;57:581.
[14] Brown SR, Scholz CH. J Geoph Res 1985;90:12.
[15] Bhushan B, Blackman G. Trans ASME J Trib 1991;113:452.
[16] Maloy KJ, Hansen A, Hinrichsen EL, Roux S. Phys Rev Lett 1992;68:213.
[17] Poon CY, Sayles RS, Jones TA. J Phys D: Appl Phys 1992;25:1269.
[18] Cox BL, Wang JSY. Fractals 1993;1:87.
[19] Doege E, Laackman B, Kischnick B. Metalworking 1995;66:113.
[20] Dohda K, Wilson SJW. Tribology in Manufactoring. In: New-York: A.S.M.E, 1994.
[21] Wilson W. J of Applied Metalworking 1979;1:7.
[22] Patir N, Cheng HS. J of Lubrication Tech 1978;100:12.
[23] Roux S, Schmittbuhl J, Vilotte JP, Hansen A. Europhys Lett 1993;23:277.
[24] Plouraboué F, Kurowski P, Hulin JP, Roux S, Schmittbuhl J. Phys Rev E 1995;51:1675.
[25] Schmittbuhl J, Vilottte JP, Roux S. Physics A 1993;26:6115.
[26] Markiewicz P, Goh MC. J Vac Sci Technol B 1995;13:1115.
[27] Bonnet N, Dongmo S, Vautrot P, Troyon M. Microanal Microstruct 1994;5:477.
[28] Leung ECW, Markiewicz P, Goh MC. J Vac Sci Technol B 1997;15:181.
[29] Tabet MF, Urban FK. J Vac Sci Technol B 1997;15:800.
[30] Villarrubia JS. Surface Science 1994;321:287.
[31] Tabary P, Sutcliffe M, Porral F, Deneuville P. J Tri 1996;118:629.
[32] Pinkus O, Sternlicht B. Theory of hydrodynamical lubrication. New York: McGraw-Hill, 1961.